Original Article

JVS

Non-invasive quantification of hepatic fat content in healthy dogs by using proton magnetic resonance spectroscopy and dual gradient echo magnetic resonance imaging

Francesca Del Chicca[1,2,*], Andrea Schwarz[3], Dieter Meier[4,5], Paula Grest[6], Annette Liesegang[7], Patrick R. Kircher[1]

[1]Clinic of Diagnostic Imaging, [3]Section of Anesthesiology, Equine Department, and Institutes of [6]Veterinary Pathology and [7]Animal Nutrition, Vetsuisse Faculty, University of Zurich, 8057 Zurich, Switzerland
[2]Graduate School for Cellular and Biomedical Sciences, University of Bern, 3012 Bern, Switzerland
[4]Institute of Biomedical Engineering, University of Zurich, 8057 Zurich, Switzerland
[5]Swiss Federal Institute of Technology (ETH Zurich), 8092 Zurich, Switzerland

The objective of the present study was to describe two non-invasive methods for fat quantification in normal canine liver by using magnetic resonance imaging (MRI) and spectroscopy. Eleven adult beagle dogs were anesthetized and underwent magnetic resonance examination of the cranial abdomen by performing morphologic, modified Dixon (mDixon) dual gradient echo sequence, and proton magnetic resonance spectroscopy (^{1}H MRS) imaging. In addition, ultrasonographic liver examination was performed, fine-needle liver aspirates and liver biopsies were obtained, and hepatic triglyceride content was assayed. Ultrasonographic, cytologic, and histologic examination results were unremarkable in all cases. The median hepatic fat fraction calculated was 2.1% (range, 1.3%–5.5%) using mDixon, 0.3% (range, 0.1%–1.0%) using ^{1}H MRS, and 1.6% (range 1.0%–2.5%) based on triglyceride content. The hepatic fat fractions calculated using mDixon and ^{1}H MRS imaging were highly correlated to that based on triglyceride content. A weak correlation between mDixon and ^{1}H MRS imaging was detected. The results show that hepatic fat content can be estimated using non-invasive techniques (mDixon or ^{1}H MRS) in healthy dogs. Further studies are warranted to evaluate the use of these techniques in dogs with varying hepatic fat content and different hepatic disorders.

Keywords: canine, hepatic triglyceride, liver, magnetic resonance imaging, proton magnetic resonance spectroscopy

Introduction

Intracellular fat accumulation in the liver is a common feature of many liver disorders, and hepatic steatosis is widely recognized in humans as the most prevalent cause of liver disease and a contributing factor in the progression of chronic hepatic disorders [18,28]. Hepatic steatosis (lipidosis) is also observed in dogs and cats and is associated with obesity, diabetes, prolonged fasting, congenital portosystemic shunts, endocrinopathy, and toxic liver injury [4]. Consequently, diagnostic tools to reliably detect and grade hepatic fat accumulation have been much sought after in human medicine and may prove useful in veterinary medicine [33]. Liver biopsy, the current gold standard, is invasive, provides evaluation of only 0.002% of the liver, is subject to inter-observer variability,

and is associated with a risk of bleeding [2,18]. Ultrasound can detect moderate to marked fatty infiltration of the liver but other diffuse hepatic disorders may have similar sonographic appearances, and interpretation is operator-dependent [6,8,9, 13,16]. Moreover, quantitative methods based on histogram analysis only grade echogenicity, which is non-specific for fatty infiltration, and inapplicable in routine practice [5,8]. Computed tomography has been evaluated in humans and cats for the diagnosis of hepatic lipidosis but is unreliable at quantifying fatty infiltration when concurrent hepatic parenchymal disease exists [14,21].

Dual gradient echo magnetic resonance imaging (DGE-MRI) is considered one of the most sensitive modalities for the detection of fatty infiltration of the liver in humans [2]. This technique uses chemical shift imaging, taking advantage of the

different precession frequencies of fat and water protons in a magnetic field. Different echo-time parameters are used such that the signal from fat protons is either in phase (IP) or in opposed phase (OP) with that of water protons. The derived signals are those of fat and water added together (IP) or water minus fat signal (OP) [20]. Using this principle, the modified Dixon (mDixon) imaging method uses a reconstruction algorithm from which the fat fraction is derived from the difference in IP and OP signal intensities on a pixel-by-pixel basis, producing water only, fat only, IP, and OP images via fast gradient echo sequencing [18].

Proton magnetic resonance spectroscopy (^{1}H MRS) records signals from protons embedded in different chemical bonds within a given volume of tissue, with the bonds identified by their spectral frequencies. As protons are surrounded by nuclei and electrons with their own magnetic properties, slight differences occur in the received frequencies from protons in different chemical bonds. The spectral position of resonances, due to these chemical shifts, is expressed in parts per million (ppm) relative to a reference set at 0 ppm. At field strengths at or above 1.5 T, the frequency peaks of lipid and water protons are approximately 1.2 ppm and 4.7 ppm, respectively [18].

As ^{1}H MRS can distinguish spectral frequencies of protons in water from those in fatty acids, the fat signal fraction can be calculated, providing an accurate measure of hepatic fat compared to estimates from biopsy or chemical triglyceride assays [3,18,29]. Previous studies have described hepatic fat quantification using ^{1}H MRS in humans [18], lean and obese cats [3], and rats [26], as well as in a study of experimentally-induced hepatic fat accumulation in dogs and rabbits [29]. In lean and obese cats, the median liver fat percentages measured by applying ^{1}H MRS were 1.3% and 6.8%, respectively [3]. To the authors' knowledge, hepatic fat content in lean or obese dogs has not, thus far, been quantified by using DGE-MRI or ^{1}H MRS techniques.

The objective of this prospective sample survey study was to explore the feasibility of hepatic fat quantification by using DGE-MRI and ^{1}H MRS in healthy adult dogs and to compare fat quantification derived via these techniques with results from histological and cytological examination, which represent the standard diagnostic approach in clinical patients. The use of the investigated techniques in a clinical setting may be of potential benefit in non-invasive diagnosis and monitoring of canine patients.

Materials and Methods

Ethical approval

All procedures involving the dogs in this study were approved by the Cantonal Veterinary Office of Zurich (approval No. 114/2013).

Dogs

Eleven research purpose-bred dogs (5 females and 6 males) were used in the study. The dogs had a mean age of 4.1 years (range, 3.4–6 years) and a mean body weight of 13.6 kg (range, 10.0–15.0 kg). The dogs had a median body condition score (BCS) of 7/9 (range, 6–8). The dogs were deemed healthy based on physical examination, complete blood count, and biochemistry profile results.

Anesthesia

Dogs were anesthetized following a standard protocol. This included premedication with methadone (0.2 mg/kg) followed, 30 min later, by midazolam (0.1 mg/kg intravenous [IV]) administered via a cephalic catheter. Anesthesia was induced, to effect, with propofol. Following endotracheal intubation, anesthesia was maintained by using sevoflurane delivered in an oxygen/air mixture with a flow of 50 mL/kg/min and an inspired fraction of oxygen of 0.5. Dogs were mechanically ventilated by using a breathing system in volume-cycled mode to maintain an end-tidal PCO_2 of 35 mmHg. Lactated Ringer's solution (5 mL/kg/h) was administered IV throughout anesthesia. Monitoring included continuous assessment of heart and respiratory rates, pulse oximetry, body temperature, and end-tidal PCO_2, as well as intermittent oscillometric non-invasive blood pressure measurements. If mean arterial pressure was below 60 mmHg, the inspired fraction of sevoflurane was decreased by 0.5% and an IV fluid bolus (2 mL/kg) of lactated Ringer's solution was administered. If hypotension persisted, a constant rate infusion of IV dobutamine (initial dose, 2 μg/kg/h) was administered.

Magnetic resonance imaging and spectroscopy

The dogs were placed in dorsal recumbency in a 3 T scanner (Philips Ingenia 3.0 T scanner; Philips Healthcare, Switzerland) with a phased-array anterior coil (dStream body coil solution, 32 channels; Philips Healthcare). Initial transverse cranial abdominal sequences were performed to rule out hepatic morphologic abnormalities by obtaining T2-weighted (turbo spin echo; repetition time, 1,250 msec; echo time, 80 msec; flip angle, 90°; field of view, 220 mm; voxel size, 0.60 mm × 0.73 mm × 3.00 mm; slice thickness, 3.00 mm; slice gap, 0.5 mm) and T1-weighted pre- and post-contrast scans.

For breath-hold sequences (both DGE-MRI and ^{1}H MRS sequences), mechanical ventilation was interrupted to allow brief expiratory apnea (maximal scan length, 28 sec) and resumed immediately thereafter. The DGE-MRI sequence was performed on the cranial abdomen via a transverse scan (3D T1-weighted, fast dual gradient echo; repetition time, 3.6 msec; echo times, 1.2 msec [OP] and 2.3 msec [IP]; field of view, 280 mm × 280 mm × 165 mm; voxel size, 1.5 mm × 2.5 mm × 1.5 mm; number of excitations, 1). Hepatic ^{1}H MRS spectra were obtained by using a multi-echo single shot technique (point resolved spectroscopy, PRESS) on a single voxel (volume, 20

mm^3) of the liver (echo time, 38 msec; recovery time, 2,000 msec; number of signal averages, 12; spectral bandwidth, 2,000 Hz; flip angle, 90°) using pencil-beam automatic shimming. The voxel to be analyzed was selected based on the T2-weighted and DGE-MRI sequences in order to avoid blood vessels, gallbladder, and fatty tissue.

Finally, gadodiamide contrast (Gadodiamid [Omniscan], 0.3 mmol/kg; GE Healthcare, Switzerland) was administered IV by using an automatic injector (2 mL/sec), followed by a 10 mL saline flush. An enhanced T1 high-resolution isotropic volume excitation (e-Thrive) sequence was performed by using turbo field echo, and SENSE (dynamic parallel imaging performance sensitivity) encoding was performed (repetition time, 3.1 msec; echo time, 1.5 msec; flip angle, 10°; field of view, 280 mm; voxel size, 1.49 mm × 1.51 mm × 3.00 mm; slice thickness, 3 mm; slice gap, −1.5 mm; number of dynamics, 6). The scan was manually started when contrast enhancement was visible in the descending aorta in the pre-monitoring window and was repeated 6 times consecutively.

Ultrasound and tissue sampling

Following the MRI and spectroscopy procedures, and during the same anesthesia session, dog livers were examined by using ultrasound (Philips iU22 Ultrasound system; Philips Healthcare) applied by a single examiner (F. Del Chicca). Two ultrasound-guided fine-needle (22 gauge) aspirates and two ultrasound-guided needle biopsies (Tru-cut, 16 gauge) using an automatic biopsy gun were obtained.

Subsequently, the dogs recovered from anesthesia following IV methadone (0.2 mg/kg) administration and were monitored for 2 to 4 h in the intensive care unit. Finally, a follow-up abdominal ultrasound was performed to evaluate the abdomen for possible signs of a bleeding complication.

Tissue processing analysis

All cytologic and histologic samples were assessed by a single board-certified pathologist (P. Grest) blinded to the imaging outcomes. Cytologic samples were stained with a modified Wright's stain. Biopsies from 7 of the 11 dogs were fixed in 4% buffered formaldehyde and embedded in paraffin. Sections (4 μm thick) were cut and routinely stained with hematoxylin and eosin. In formalin-fixed, paraffin-embedded tissue, fat presents as velar, empty, variable-sized vacuoles. Hepatocytes were evaluated for the presence of microvesicular changes characterized by numerous uniform intracytoplasmic vacuoles that are smaller than the centrally located nucleus or for macrovesicular changes with vacuoles the size of the nucleus or larger and, frequently, with a displaced nucleus. Biopsies from the remaining 4 dogs were used for the biochemical assays. This was done by extracting lipids by applying a modified Foch method. Briefly, 1 mL chloroform/methanol (2:1) was added to 50 mg fresh liver followed by homogenizing in a bead mill (30 Hz, 4 × 30 sec). The homogenate was centrifuged (5 min) to separate the upper phase (aqueous methanol dragging) and lower phase (chloroform) containing lipids. The upper phase was removed by siphoning, which was repeated after rinsing the interface between phases twice with methanol/water (1:1) without mixing. The lower chloroform phase was evaporated under vacuum, resuspended in 50 μL DMSO, and shaken for 20 min at 37°C. Finally, triglyceride level was measured by using a commercial enzymatic colorimetric kit (Diatools Trig; Diatools, Switzerland) on a biochemistry analyzer (Cobas Mira; Roche Diagnostics, Switzerland).

Postprocessing and data analysis

Postprocessing of magnetic resonance data was conducted on a dedicated workstation (Extended MR WorkSpace, ver. 2.6.3.5; Philips Medical Systems, The Netherlands).

On DGE-MRI sequences, 3 regions of interest (ROIs) that avoided large vessels and organ boundaries were drawn in the liver parenchyma (Fig. 1). The signal intensity (SI) in IP and OP phase images was recorded and the hepatic fat fraction (HFF) was calculated as [SI(IP) − SI(OP)] / [2 × SI(IP)] [18]. For data analysis, the average of 3 calculated HFF values was used.

The relative proton densities of fat and water were calculated from ^{1}H MRS spectral data by using an automated fitting method (LCModel, ver. 6.3-0B; Stephen Provencher, Canada) [23]. The fitting algorithm for liver analysis provided estimates for all lipid signals. For hepatic fat quantification, the ratio between the fat signal peaks and the sum of the fat and water peaks was calculated [fat signal peak / (fat signal peak area + water peak area)] (Fig. 2). The ratio was corrected for different T1 times of water and fat in relation to the applied repetition time (2,000 msec).
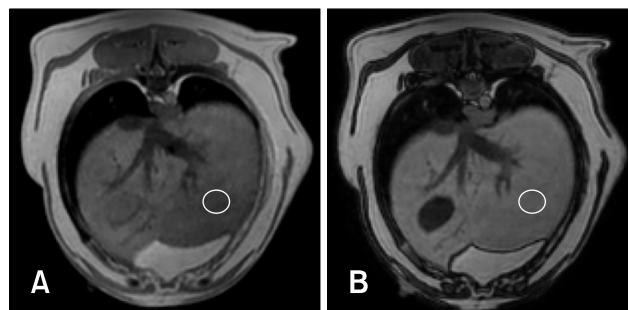
Fig. 1. Representative example of the appearance of a normal liver in the in-phase (A) and opposed-phase (B) imaging from dual gradient echo magnetic resonance imaging sequences. A regions of interest drawn in the left caudal parenchyma is shown (circles). The signal intensity is similar on both images and the mean calculated hepatic fat fraction was 1.1%.
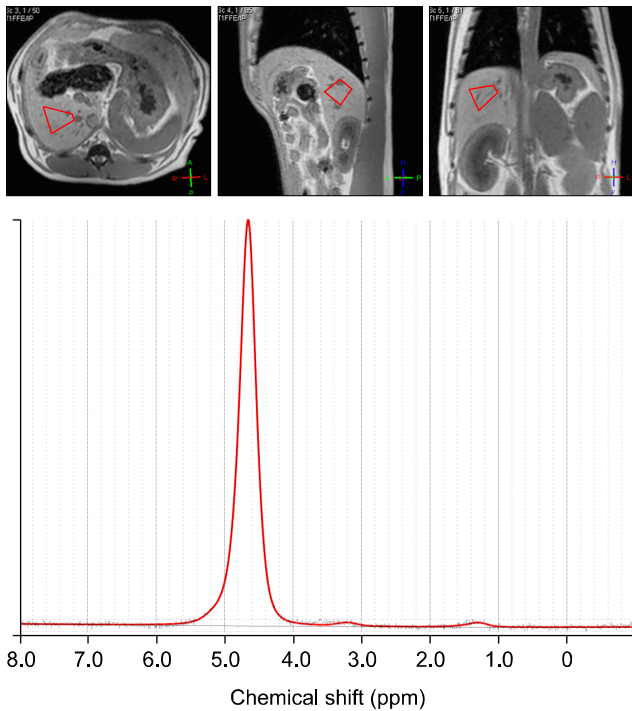
Fig. 2. Representative proton magnetic resonance spectroscopy spectrum of the dog from Fig. 1 showing the corresponding transverse (left image), sagittal (middle image) and dorsal (right image) localizing scans and the voxel placement (red polygon). On the graph, the x-axis indicates the chemical shift in parts per million (ppm). The highest peak, at the 4.6 ppm position, corresponds to the water peak. The smaller peak at the 1.2 ppm, corresponds to the lipid peak. The calculated hepatic fat fraction was 0.63%.

Statistical analysis

Statistical analysis was performed by using a commercial software package (IBM SPSS Statistics for Windows, ver. 21.0, 64-bit edition; IBM, USA). Descriptive statistics were obtained and hepatic triglyceride concentration results from biochemical analysis and HFF, calculated with DGE-MRI and ^{1}H MRS, were compared. Correlation between measurements was assessed by using Spearman's rank correlation with significance set at $p < 0.01$. For interpretation of the strength of an association, rank correlation (r_s) values of 0.8 to 1.0 were regarded as very strong, 0.6 to 0.79 as strong, 0.4 to 0.59 as moderate, 0.2 to 0.39 as weak, and 0 to 0.19 as very weak.

Results

The results of ultrasonographic examinations of liver and gallbladder were considered unremarkable in echogenicity and structures in all dogs. Likewise, cytologic and H&E stained histologic samples revealed no abnormalities or intracytoplasmic lipid vacuoles in any of the dogs. Histologic samples stained
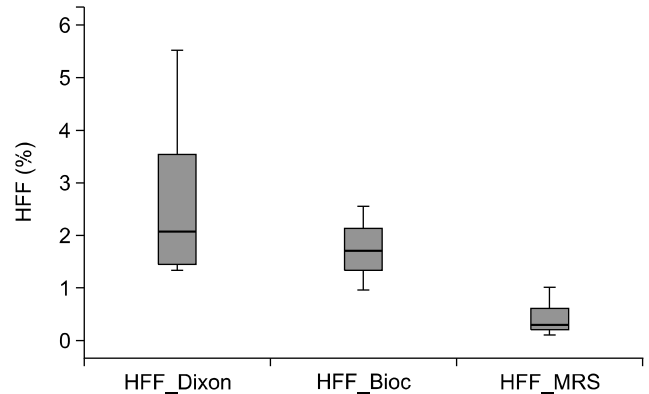
Fig. 3. Box plots of hepatic fat fraction (HFF) measured by using dual gradient echo magnetic resonance imaging (modified Dixon), proton magnetic resonance spectroscopy (MRS), and biochemical analysis (Bioc).

with Oil Red O revealed small ($<$ 1 μm) lipid droplets within hepatocytes and bile ducts. Hepatic MRI morphology was considered unremarkable with homogeneous hyperintense signals compared to the epaxial musculature and hypointense signals compared to the spleen on T2-weighted images, as well as homogeneous and mildly hyperintense signals compared to the epaxial musculature on T1-weighted mages. The mean length of the T2-weighted sequences was 6.2 ± 2.9 min, while that of DGE-MRI sequences was of 2 min ± 30 sec. The mean length of the spectroscopy sequences was 12 ± 5 min.

The mean ± SD size of the ROIs on DGE-MRI sequences was 1.05 ± 0.04 cm^2 (Fig. 1). There was no statistically significant difference in HFF calculated from the different ROIs. The median calculated HFF was 2.1% (range, 1.3−5.5%) based on DGE-MRI (modified Dixon) sequences, 0.3% (range, 0.1−1.0%) based on ^{1}H MRS, and 1.6% (range, 1.0−2.5%) based on biochemical analysis (Fig. 3). The correlations between the biochemical analysis and HFF results based on DGE-MRI (r_s = 1.0) and ^{1}H MRS (r_s = 0.8) were very strong. However, the correlation between the HFFs based on DGE-MRI and ^{1}H MRS analysis was weak (r_s = 0.34).

Discussion

The present study evaluated two imaging techniques to quantify HFF in dogs and to determine their potential as alternative methods to invasive procedures for the diagnosis, grading, and/or monitoring of hepatic steatosis. To the authors' knowledge, non-invasive techniques for hepatic fat quantification in healthy dogs have not been previously described.

A suspicion of hepatic steatosis may be aroused by observation of diffusely increased echogenicity when using ultrasound. However, increased echogenicity is not specific for fatty infiltration and has been described in association with a number

of other parenchymal disorders [9,12]. Therefore, a definitive diagnosis is generally only possible by sampling hepatic tissue, but such sampling is invasive, carries a risk of bleeding, and only allows evaluation of small amount of tissue. Moreover, the distribution of the steatosis may be uneven throughout the liver, and the region sampled may not be representative of the severity of the disease.

In humans, HFF using DGE-MRI or ^{1}H MRS has been shown to have greater correlation with histopathologic examination results than those from ultrasound or computed tomographic examination [15,28,31]. In healthy humans, the HFF using ^{1}H MRS was reported to be 1.9%, and a cut off of 5.6% has been proposed for the diagnosis of hepatic steatosis [30]. Other studies have shown that DGE-MRI yields HFF values comparable to quantitative fat measurements from biopsies [11,19] and ^{1}H MRS measurements [1,10]. Moreover, one study showed that HFF based on DGE-MRI was the most accurate method for the diagnosis of hepatic steatosis compared to results from other non-invasive imaging techniques [15].

On morphological MRI images the liver of all dogs was considered to have normal signal intensity [7]. Data from the present study suggest that DGE-MRI is also valid for estimation of HFF in canine livers as it provided a high correlation with the biochemical fat quantification estimates. Given that DGE-MRI is fast, it is relatively insensitive to motion artifacts and requires only a short apnea. Moreover, it allows evaluation of images from the entire parenchyma, reducing the risk of unrepresentative sampling due to variation in the distribution of histopathologic lesions [13]. SI loss on IP images may, however, result from excessive hepatic iron accumulation [32], which was excluded in dogs in the present study based on histopathologic examinations. As all dogs in the present study were healthy animals, further studies are required to assess the usefulness of DGE-MRI and ^{1}H MRS in dogs with hepatic disease.

In humans, ^{1}H MRS was reported to have a high correlation ($r_s = 0.876$) with hepatic lipid content [25,27] in non-alcoholic fatty liver disease. Data from the present study shows a strong correlation between ^{1}H MRS and biochemical analysis results, similar to that reported in humans [25]. However, HFF based on ^{1}H MRS underestimated HFF in the present study, as was also previously observed in a study in mice with moderately elevated hepatic fat content [26].

Previous studies have shown a greater correlation between HFF based on ^{1}H MRS and histology in rats with severe steatosis than that in those with only moderate steatosis [17] suggesting an increase in correlation with increasing fat content. As a consequence, ^{1}H MRS may perform better when estimating HFF than the data from our study in healthy lean dogs suggest. The PRESS sequence was used in the present study, which has a higher signal-to-noise ratio than other spectroscopy sequences [22,24], although it allows measurements of only 2 of a possible 6 lipids resonance peaks. As one of the minor lipid peaks overlaps with the water peak [22], and cannot be quantified with the PRESS sequence, this may have produced some degree of underestimation of HFF with ^{1}H MRS in the present study.

Disadvantages of ^{1}H MRS include high sensitivity to motion artifacts, thus a breath holding or gating technique is mandatory. The highly variable length of this sequence in each dog depended on the compensation time between subsequent apneas. With another kind of triggering, such as gating, it is likely that the sequence length would have been shorter and more uniform among the dogs.

In ^{1}H MRS sequences only a small region of hepatic parenchyma is evaluated. The technique provides spectra for a small sub-region of the liver parenchyma and, in order to obtain a spectrum of good quality, the voxel should not be in contact with organ boundaries, blood vessels, or biliary structures. Thus, mainly in smaller dogs, there may be only limited possibilities for voxel placement, and the voxel may not necessarily match the region with the most severe pathology. In the dogs we examined, even if the major hepatic vessels were avoided, the voxel may have likely included smaller blood vessels. As the placement of the voxel was based on previous MRI sequences acquired some minutes earlier, slight motion of the diaphragm may have caused some degree of spatial mismatch. This may, at least in part, explain the weak correlation found between the HFFs estimated using DGE-MRI and ^{1}H MRS.

Neither of the two imaging techniques used in the present study can be used to discriminate between microvesicular and macrovesicular hepatic steatosis or to show the histologic distribution of lipid accumulation, but both may provide non-invasive anatomic and semi-quantitative information without the use of ionizing radiation or the need for contrast media. Moreover, both of the described techniques require adequate software. For the ^{1}H MRS, additional LCModel software and expertise in this field are necessary for the correct post-processing and data interpretation.

In contrast to human medicine, veterinary medicine MRI examination requires general anesthesia. This may encounter some clinical resistance because of the intrinsic risk for the patient, as well as time and costs issues. On the other hand, the possibility of non-invasive diagnosis and monitoring of patients is attractive and should be investigated.

One major limitation of the present study was the small number of animals examined. This greatly limits the validity of the measured correlations; thus, further studies are necessary to evaluate the use of these techniques in dogs with varying degree of hepatic lipid accumulation. A further limitation was that the region of liver sampled for biopsy was differed among the dogs and did not correspond to the ROI of the DGE-MRI images or to the voxel of the ^{1}H MRS. As dogs included in the present study were lean healthy dogs with minimal hepatic fat, as

measured by using any technique, this is unlikely to have greatly affected the results, but it may be a confounder in future studies of dogs with hepatic disorders exhibiting non-uniform distribution of fat accumulation.

In conclusion, herein, we report the first use of DGE-MRI and ^{1}H MRS to estimate HFF in dogs. Unremarkable cytologic and histologic sample results in dogs with a mean BCS of 7/9 corresponded with the reported HFF values obtained using the two described techniques. There was a tendency for ^{1}H MRS to underestimate HFF. Further studies in dogs in different body condition and with varying hepatic lipid content are necessary for further evaluation and validation of both techniques and for consideration as future diagnostic applications.

Conflict of Interest

The authors declare no conflicts of interest.

References

1. **Borra RJ, Salo S, Dean K, Lautamäki R, Nuutila P, Komu M, Parkkola R.** Nonalcoholic fatty liver disease: rapid evaluation of liver fat content with in-phase and out-of-phase MR imaging. Radiology 2009, **250**, 130-136.
2. **Chandarana H, Taouli B.** Diffusion and perfusion imaging of the liver. Eur J Radiol 2010, **76**, 348-358.
3. **Clark MH, Larsen R, Lu W, Hoenig M.** Investigation of ^{1}H MRS for quantification of hepatic triglyceride in lean and obese cats. Res Vet Sci 2013, **95**, 678-680.
4. **Cullen JM, van den Ingh TSGAM, Van Winkle T, Charles JA, Desmet VJ.** Morphological classification of parenchymal disorders of the canine and feline liver: 1. Normal histology, reversible hepatocytic injury and hepatic amyloidosis. In: WSAVA Liver Standardization Group, Rothuizen J, Bunch SE, Charles JA, Cullen JM, Desmet VJ, Szatmári V, Twedt DC, van den Ingh TSGAM, Van Winkle T, Washabau RJ (eds.). WSAVA Standards for Clinical and Histological Diagnosis of Canine and Feline Liver Disease. pp. 77-83, Elsevier, Philadelphia, 2006.
5. **Drost WT, Henry GA, Meinkoth JH, Woods JP, Lehenbauer TW.** Quantification of hepatic and renal cortical echogenicity in clinically normal cats. Am J Vet Res 2000, **61**, 1016-1020.
6. **Feeney DA, Anderson KL, Ziegler LE, Jessen CR, Daubs BM, Hardy RM.** Statistical relevance of ultrasonographic criteria in the assessment of diffuse liver disease in dogs and cats. Am J Vet Res 2008, **69**, 212-221.
7. **Feeney DA, Sharkey LC, Steward SM, Bahr KL, Henson MS, Ito D, O'Brien TD, Jessen CR, Husbands BD, Borgatti A, Modiano JF.** Parenchymal signal intensity in 3-T body MRI of dogs with hematopoietic neoplasia. Comp Med 2013, **63**, 174-182.
8. **Gaschen L.** Update on hepatobiliary imaging. Vet Clin North Am Small Anim Pract 2009, **39**, 439-467.
9. **Guillot M, Danjou MA, Alexander K, Bédard C, Desnoyers M, Beauregard G, Del Castillo JR.** Can sonographic findings predict the results of liver aspirates in dogs with suspected liver disease? Vet Radiol Ultrasound 2009, **50**, 513-518.
10. **Guiu B, Loffroy R, Petit JM, Aho S, Ben Salem D, Masson D, Hillon P, Cercueil JP, Krause D.** Mapping of liver fat with triple-echo gradient echo imaging: validation against 3.0-T proton MR spectroscopy. Eur Radiol 2009, **19**, 1786-1793.
11. **Hussain HK, Chenevert TL, Londy FJ, Gulani V, Swanson SD, McKenna BJ, Appelman HD, Adusumilli S, Greenson JK, Conjeevaram HS.** Hepatic fat fraction: MR imaging for quantitative measurement and display--early experience. Radiology 2005, **237**, 1048-1055.
12. **Kemp SD, Panciera DL, Larson MM, Saunders GK, Werre SR.** A comparison of hepatic sonographic features and histopathologic diagnosis in canine liver disease: 138 cases. J Vet Intern Med 2013, **27**, 806-813.
13. **Kemp SD, Zimmerman KL, Panciera DL, Monroe WE, Leib MS.** Histopathologic variation between liver lobes in dogs. J Vet Intern Med 2015, **29**, 58-62.
14. **Kühn JP, Evert M, Friedrich N, Kannengiesser S, Mayerle J, Thiel R, Lerch MM, Dombrowski F, Mensel B, Hosten N, Puls R.** Noninvasive quantification of hepatic fat content using three-echo dixon magnetic resonance imaging with correction for T2* relaxation effects. Invest Radiol 2011, **46**, 783-789.
15. **Lee SS, Park SH, Kim HJ, Kim SY, Kim MY, Kim DY, Suh DJ, Kim KM, Bae MH, Lee JY, Lee SG, Yu ES.** Non-invasive assessment of hepatic steatosis: prospective comparison of the accuracy of imaging examinations. J Hepatol 2010, **52**, 579-585.
16. **Marks AL, Hecht S, Stokes JE, Conklin GA, Deanna KH.** Effects of gadoxetate disodium (Eovist®) contrast on magnetic resonance imaging characteristics of the liver in clinically healthy dogs. Vet Radiol Ultrasound 2014, **55**, 286-291.
17. **Marsman HA, van Werven JR, Nederveen AJ, Ten Kate FJ, Heger M, Stoker J, van Gulik TM.** Noninvasive quantification of hepatic steatosis in rats using 3.0 T [1]H-magnetic resonance spectroscopy. J Magn Reson Imaging 2010, **32**, 148-154.
18. **Mazhar SM, Shiehmorteza M, Sirlin CB.** Noninvasive assessment of hepatic steatosis. Clin Gastroenterol Hepatol 2009, **7**, 135-140.
19. **Mennesson N, Dumortier J, Hervieu V, Milot L, Guillaud O, Scoazec JY, Pilleul F.** Liver steatosis quantification using magnetic resonance imaging: a prospective comparative study with liver biopsy. J Comput Assist Tomogr 2009, **33**, 672-677.
20. **Mitchell DG, Kim I, Chang TS, Vinitski S, Consigny PM, Saponaro SA, Ehrlich SM, Rifkin MD, Rubin R.** Fatty liver. Chemical shift phase-difference and suppression magnetic resonance imaging techniques in animals, phantoms, and humans. Invest Radiol 1991, **26**, 1041-1052.
21. **Nakamura M, Chen HM, Momoi Y, Iwasaki T.** Clinical application of computed tomography for the diagnosis of feline hepatic lipidosis. J Vet Med Sci 2005, **67**, 1163-1165.
22. **Perman WH, Balci NC, Akduman I.** Review of magnetic resonance spectroscopy in the liver and the pancreas. Top Magn Reson Imaging 2009, **20**, 89-97.
23. **Provencher SW.** Estimation of metabolite concentrations from localized in vivo proton NMR spectra. Magn Reson

Med 1993, **30**, 672-679.

24. **Qayyum A.** MR spectroscopy of the liver: principles and clinical applications. Radiographics 2009, **29**, 1653-1664.
25. **Roldan-Valadez E, Favila R, Martínez-López M, Uribe M, Ríos C, Méndez-Sánchez N.** *In vivo* 3T spectroscopic quantification of liver fat content in nonalcoholic fatty liver disease: correlation with biochemical method and morphometry. J Hepatol 2010, **53**, 732-737.
26. **Runge JH, Bakker PJ, Gaemers IC, Verheij J, Hakvoort TB, Ottenhoff R, Stoker J, Nederveen AJ.** Quantitative determination of liver triglyceride levels with 3T [1]H-MR spectroscopy in mice with moderately elevated liver fat content. Acad Radiol 2014, **21**, 1446-1454.
27. **Schwenzer NF, Springer F, Schraml C, Stefan N, Machann J, Schick F.** Non-invasive assessment and quantification of liver steatosis by ultrasound, computed tomography and magnetic resonance. J Hepatol 2009, **51**, 433-445.
28. **Springer F, Machann J, Claussen CD, Schick F, Schwenzer NF.** Liver fat content determined by magnetic resonance imaging and spectroscopy. World J Gastroenterol 2010, **16**, 1560-1566.
29. **Szczepaniak LS, Babcock EE, Schick F, Dobbins RL, Garg A, Burns DK, McGarry JD, Stein DT.** Measurement of intracellular triglyceride stores by H spectroscopy: validation

in vivo. Am J Physiol 1999, **276**, E977-989.
30. **Szczepaniak LS, Nurenberg P, Leonard D, Browning JD, Reingold JS, Grundy S, Hobbs HH, Dobbins RL.** Magnetic resonance spectroscopy to measure hepatic triglyceride content: prevalence of hepatic steatosis in the general population. Am J Physiol Endocrinol Metab 2005, **288**, E462-468.
31. **van Werven JR, Marsman HA, Nederveen AJ, Smits NJ, ten Kate FJ, van Gulik TM, Stoker J.** Assessment of hepatic steatosis in patients undergoing liver resection: comparison of US, CT, T1-weighted dual-echo MR imaging, and point-resolved ^{1}H MR spectroscopy. Radiology 2010, **256**, 159-168.
32. **Westphalen AC, Qayyum A, Yeh BM, Merriman RB, Lee JA, Lamba A, Lu Y, Coakley FV.** Liver fat: effect of hepatic iron deposition on evaluation with opposed-phase MR imaging. Radiology 2007, **242**, 450-455.
33. **Yokoo T, Shiehmorteza M, Hamilton G, Wolfson T, Schroeder ME, Middleton MS, Bydder M, Gamst AC, Kono Y, Kuo A, Patton HM, Horgan S, Lavine JE, Schwimmer JB, Sirlin CB.** Estimation of hepatic proton-density fat fraction by using MR imaging at 3.0 T. Radiology 2011, **258**, 749-759.